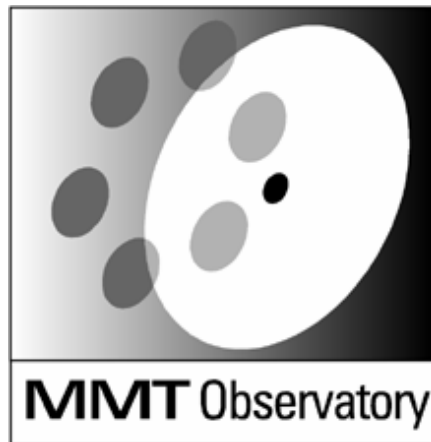


## MMTO Technical Memorandum #03-6



Smithsonian Institution &  
The University of Arizona®

### **F/9 Top-Box Shack-Hartmann: Practical Design and Implementation**

**S. C. West, S. P. Callahan, R. James, P. Spencer,  
H. Olson, B. Kindred, R. Ortiz, T. Pickering**

March 2003

# F/9 top-box Shack-Hartmann: practical design and implementation

MMTO Technical Memo #03-6, 5 March 2003

S.C. West, S.P. Callahan, R. James, P. Spencer, H. Olson, B. Kindred, R. Ortiz, and T. Pickering  
MMT Observatory, Tucson, AZ 85721

## Abstract

*We provide practical details of the successful implementation of a Shack-Hartmann wavefront analyzer built into the f/9 top box of the 6.5m MMT. The opto-mechanical, software design, and implementation are briefly described. The optical alignment procedure within the top box is described in an Appendix.*

## I. Introduction

We describe the design and implementation of a Shack-Hartmann wavefront analyzer built into the f/9 top-box. Its hexagonal lenslet array provides 13 x 26 resolution elements within the pupil. The top-box was designed for the small field of view of the original MMT. Combined with very tight financial constraints and an uncertain future for the f/9 focus, we decided against the implementation of an xy-stage probe system for continuous monitoring like that implemented with Magellan<sup>1</sup>.

Instead we have installed the analyzer directly onto the optic axis and interrupt the science observation with a pick-off mirror for wavefront error correction. Past experience shows that wavefront errors corrected with primary mirror bending are required infrequently, and coma is corrected very well open-loop during a long observation<sup>2</sup>. The disadvantage is that accurate open-loop focus correction is difficult. It requires sophisticated temperature analysis of the optics and optical support structure (OSS). Uneven thermal loading can confound open-loop corrections. Focus correction is best done with a closed-loop servo during a long science observation.

## II. Optical design and data reduction

The optical design for the wavefront analyzer was performed with OSLO PRO (Lambda Research Corp.)<sup>3</sup>. The optical model consists of the telescope optics combined with a proposed collimator and lenslet array. A CCL script rasters a sub-aperture in the entrance pupil. The raster positions were chosen so that the sub-aperture positions and size corresponds to the projection of each lenslet onto the entrance aperture. A chief ray is drawn through each sub-aperture, and its intersection with the detector plane defines the spot centroid produced by that lenslet. All the spot centroids are saved to a file. This detailed model has the advantage of producing realistic spot diagrams that include distortion and other aberrations that would be present in the as-built system. Telescope aberrations were injected into the model by re-positioning the secondary mirror and/or adding Zernike phase error surfaces to the entrance aperture.

A C-program (getShackZernikes.c) is used to back-calculate the wavefront phase error from the files of spot centroids. The spot displacements of a “perfect” telescope combined with the proposed Shack-Hartmann optics provides the instrumental wavefront error for subtraction (*i.e.*, simulated spot diagram obtained with a reference pinhole light-source). Histograms of spot displacements are used to estimate the required accuracy of the centroiding algorithm for various optical aberrations. For example, the histograms shown in that memo indicate that a centroiding accuracy < 0.04 pixel is required to detect ~10nm of astigmatism or coma (assuming 20 micron pixels and using the p-v histogram displacements). This corresponds to a centroiding accuracy < 0.4% of the diffraction spot diameter produced by the lenslet (~200 microns).

For N wavefront polynomials  $Z_i$ , and M lenslets with dimensionless coordinates  $(x_j, y_j)$ , a relationship between the spot displacements and the wavefront polynomial gradients is given by:

$$\begin{bmatrix} \frac{\partial Z_1}{\partial x} \Big|_{x_1, y_1} & \dots & \frac{\partial Z_N}{\partial x} \Big|_{x_1, y_1} \\ & \dots & \\ & \dots & \\ \frac{\partial Z_1}{\partial x} \Big|_{x_M, y_M} & \dots & \frac{\partial Z_N}{\partial x} \Big|_{x_M, y_M} \\ \frac{\partial Z_1}{\partial y} \Big|_{x_1, y_1} & \dots & \frac{\partial Z_N}{\partial y} \Big|_{x_1, y_1} \\ & \dots & \\ & \dots & \\ \frac{\partial Z_1}{\partial y} \Big|_{x_M, y_M} & \dots & \frac{\partial Z_N}{\partial y} \Big|_{x_M, y_M} \end{bmatrix} \begin{bmatrix} C_1 \\ \dots \\ C_N \end{bmatrix} = \begin{bmatrix} \frac{\partial W_1}{\partial x} \\ \dots \\ \dots \\ \frac{\partial W_M}{\partial x} \\ \frac{\partial W_1}{\partial y} \\ \dots \\ \dots \\ \frac{\partial W_M}{\partial y} \end{bmatrix} \quad (1)$$

where  $C_i$  are the N wavefront polynomial amplitude coefficients,  $(\partial W_j)/\partial(x, y)$  are total measured wavefront gradient coefficients for the M lenslets (proportional to the measured spot motion in the x and y directions). Each column in the matrix describes the influence one polynomial gradient has on

the total wavefront gradient. The equation has the form of  $[A](x) = (b)$ , where  $[A]$  is a  $2M \times N$  matrix. We solve for the polynomial coefficients  $(x)$  using singular value decomposition (SVD). The polynomial wavefront expansion is detailed in appendix A of the report on the interferometric wavefront analyzer (previously built for the f/9 MMT focus<sup>4</sup>). The polynomials were obtained from the book Optical Shop Testing -- edition II.

The relationship between the measured wavefront errors and the axial correction force distribution of the primary mirror has been previously documented<sup>5,6</sup>. An excellent in-depth summary of Shack-Hartmann wavefront sensing and active optics is found in the recent literature<sup>7</sup>.

### III. Software

The software is designed with a scripted GUI (written in TCL/TK) wrapping stand-alone C-routines. The compiled C gives the package computational speed, while the GUI provides for flexible user control, data flow management, and graphical representation of the results. Since the core calculations are contained in the C-code, the analysis software can run independent of the GUI for control automation (*e.g.*, closing the loop).

The software can be checkout out via cvs with:

```
cvs -d rutherford:/u1/swestCVSarchive checkout shwfs
```

Figure 1 shows the software flow diagram. Data collection is done with a separate program purchased from Clearsky Institute (Elwood Downey's CAMERA program). Once the FITS images are collected, the shwfs.tcl program is used to select images and analyze the wavefront errors.

Shwfs.tcl consists of three toplevel windows. The main control window (Figure 2), processes the selection of FITS image(s) automatically through the entire data reduction pipeline shown in Figure 1. The results window (Figure 3) provides the user with graphical feedback of the wavefront errors and primary mirror correction forces. The Zernike amplitude display window shown in Figure 4 provides a tabular list of wavefront error amplitudes, allows for saving results to a log file, and provides action buttons for correcting collimation and primary mirror figure.

Appendix A lists the system call to IRAF STARFIND and the parameters used for efficient centroiding of typical spots.

### IV. Opto-mechanical design and implementation

The Shack-Hartmann optical path was built onto a Newport X-26 optical rail system (Figure 5). A second X26 rail currently holds a 1:1 focal plane reimager which is co-focal with the focus of the Shack-Hartmann lenses and the telescope

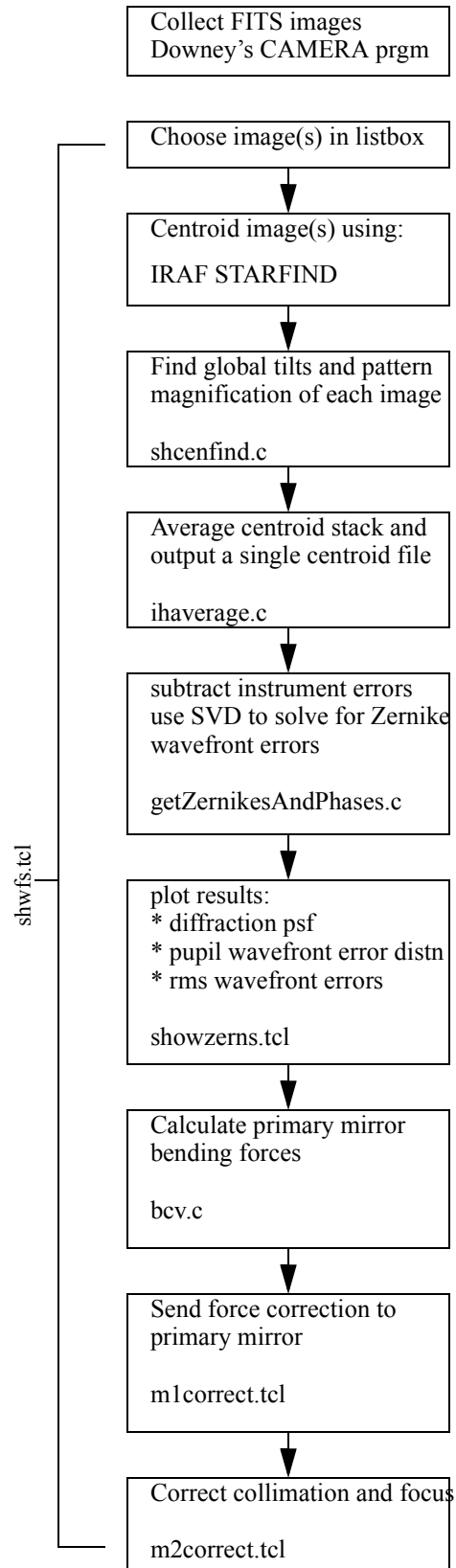


Figure 1: Flow diagram of the software listing the function and routine names for each task(s). All C-functions use the numerical recipes syntax and functions.

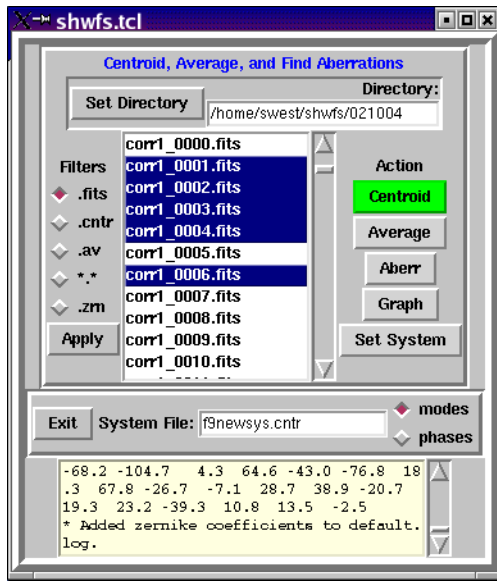


Figure 2: shwfs.tcl main window. The listbox allows discontinuous selections of the file types given by the filter radiobuttons. A pop-down window allows selection of the data directory. The System File contains the instrument error centroids and is chosen with the Set System action. Pressing the Centroid action automatically performs the entire data reduction for the selected FITS images. The other actions are subsets for engineering purposes.

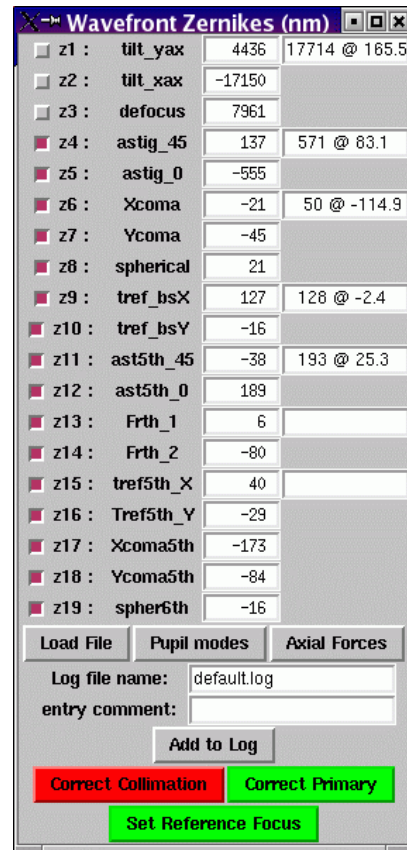


Figure 4: The wavefront error polynomial amplitudes (nm) are shown in this shwfs.tcl toplevel window. Checkbuttons allow a selection of wavefront errors to be used for display and calculating primary mirror bending forces. There is a facility to keep track of all results in a log file. Additionally, the lower buttons allow the selection of a Zernike focus reference, downloading coma and focus error to the hexapod, and the sending of primary mirror correction forces to the mirror support VxWorks system.

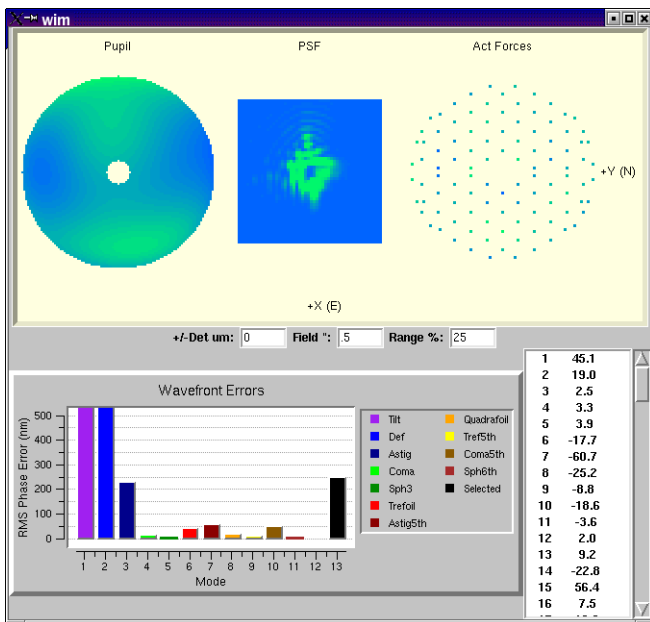


Figure 3: The results display window of shwfs.tcl. The upper three figures are pupil error distribution (left), diffraction psf, and primary mirror correction force distribution. The central three entry boxes allow fine tuning of the psf image with: detector defocus, field of view, and intensity range to show. At the bottom, there is an rms wavefront error barchart and a scrolling window to view the primary mirror correction forces prior to downloading them to the mirror support computer.

focal plane, so the CCD need not be moved when selecting either light path. The optical path is selected by actuating one axis of an Aerotech XY motorized slide.

Motorized focus is provided with the other axis of the same XY table. Mechanical focus is used only if the instrument is not mounted at the nominal  $f/9$  focus (9 inches below the top box). The Shack-Hartmann optics can accommodate up to  $\pm 3$  arcsec of focus error before either: 1) the telescope must be refocused, or 2) the wavefront sensor must be refocused. Therefore, the instrument should be mounted to the nominal  $f/9$  focus to better than  $\pm 5mm$  to operate without adjusting the focus adjustment of the wavefront analyzer. Also note, because the OSS focus error vs. elevation exceeds 6 arcsec, elevation correction of focus must be used if the wavefront sensor is needed (e.g., elcoll.tcl must be running)<sup>2</sup>.

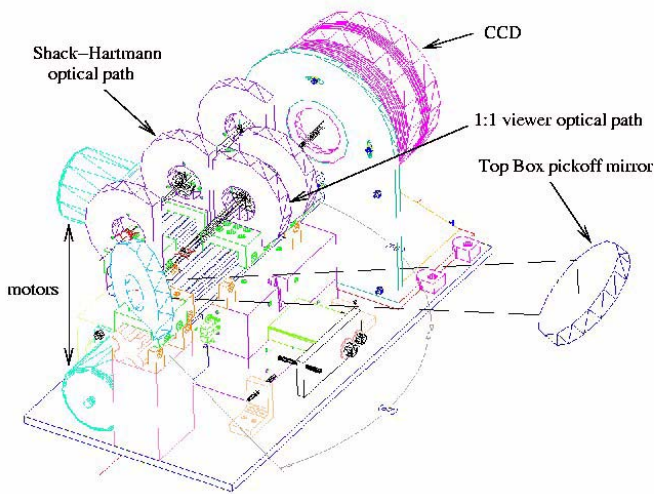


Figure 5: Mechanical drawing of the f/9 top box Shack-Hartmann assembly. There is provision for motorized selection of either the reimager or the Shack-Hartmann optical paths.

The entire unit is installed in the North section of the top box lower level. A removable pickoff mirror is stacked on top of the spectrograph comparison source assembly (so no mechanical assemblies or control electronics needed to be added to the top box). The telescope operator simply directs the spectrograph comparison assembly into the beam when the wavefront sensor is to be used. An added benefit of this arrangement is that the spectrograph comparison lamps may be used at the same time that wavefront analysis is ongoing. Figure 6 shows an image of the final instrument just before it



Figure 6: The as-built f/9 Shack-Hartmann wavefront analyzer prior to installation in the top box.

was mounted in the top box. The procedure used to align the

wavefront sensor onto the derotator axis is described in Appendix B.

Figure 7 shows spot diagrams from both a laser reference light

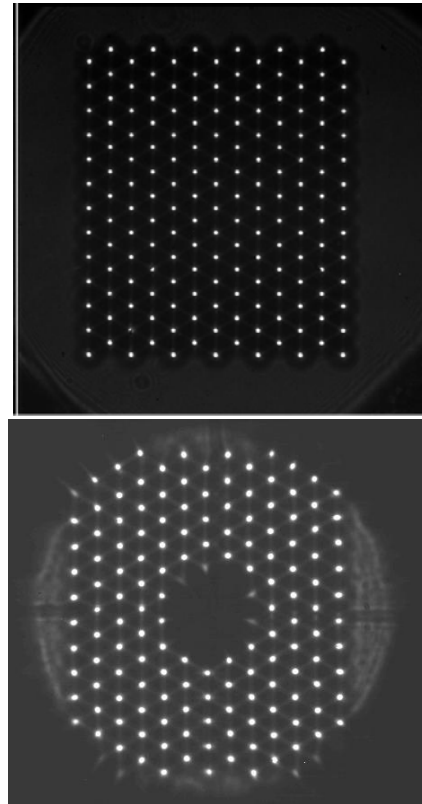


Figure 7: Images of spot diagrams produced with a pinhole reference source (top) and through the telescope. The underfilled pupil due to the rectangular lenslet array does not affect the wavefront error calculation but does aid in alignment of the lenslet on the pupil.

source and a star imaged through the telescope. The lenslet array is an Adaptive Optics Associates 625-45-H (13 x 13 format, focal length of 45 mm). The collimator is a Melles Griot 01 LAO 111 (80 mm focal length with 18 mm diameter). The CCD is an Apogee KX-260 (512 x 512 with 20 micron pixels). There is a blue cutoff filter at the pupil (RG 610). Together, the CCD and filter effective wavelength is 780 nm. In practice, a 9.3 mag K star almost fills the CCD pixels in a 30-sec. exposure near zenith in good seeing. The remaining mechanical problem is that the top box pickoff mirror assembly (shown in Figure 5) is mounted to the original spectrograph comparison mirror. The extra mass we've added causes the original top box kinematic mount to become decoupled thus misaligning both the comparison comparison source feed and the wavefront sensor beam. Recently, we have placed a couple mechanical constraints on the kinematic mount. Whether these work, time will tell. A better solution is to re-design the kinematic mount and re-align the wavefront sensor.

## V. Conclusion

We briefly describe the practical details of the Shack-Hartmann wavefront sensor built into the f/9 top box. The optical design was briefly described. Equation 1 illustrates how the measured spot motions are fit to the differentiated Zernike polynomials. The routines required for operation were presented with the software flow chart. Pictures of the three main GUI components are shown and briefly described. The mechanical assembly and picture of the finished wavefront sensor are shown along with a description of the actual components built into the unit. Appendices explain the IRAF STARFIND parameters and the procedure used to align the wavefront sensor in the f/9 top box.

The performance and usage of the wavefront sensor are described in another MMT Technical Memo<sup>2</sup>.

## VI. Acknowledgements

We thank Cory Knop, Brian Comisso, and Ken Vanhorn for electronics support with the top box. The telescope operators (Mike Alegria, Ale Milone, and John McAfee) have been very helpful supporting the initial observations with the instrument. Dennis Smith provided new tires for the top box to alleviate shock when the unit is rolled over floor irregularities. Court Wainwright and Steve Bauman provided support in mechanical drafting and design.

## VII. Appendix A: IRAF STARFIND parameters

### A. Script that makes a system call to STARFIND

```
#!/iraf/irafbin/bin.redhat/cl.e -f
# Usage: ./starfind input reference coords <other params...>
# basically, this is just a shell wrapper to run imcentroid from
any shell prompt with all command-line params passed to it
verbatim.
#define these to match desired environment so params get
saved and stuff.
# it works fine without them, though.
sethome= "/home/swest/"
#setimdir= "HDR$pixels/"
setuparm= "home$uparm/"
setuserid= "swest"
set arch = ".redhat"

set imtype = "fits"
logver = "IRAF V2.11 May 1997"
keep
images
keep
{
printf("starfind %s\n", args) | cl()
logout
}
```

### B. STARFIND parameters currently used

hwhmpsf	3.0
thresh	2000
datamin	indef
datamax	16,000
fradius	3.0
sepmin	8
npixmin	5
maglo	indef
maghi	indef
roundlo	0
roundhi	1
sharplo	0.2
sharpfi	2.0
wcs	-
wxform	-
wforma	-
boundary	nearest
constan	0
nxblock	indef
nyblock	256

## VIII. Appendix B: Aligning the wavefront sensor to the derotator axis.

This appendix documents the procedure used to align the wavefront sensor to the telescope derotator axis. The f/9 top box is mounted so that its mechanical axis is nearly coincident with the telescope derotator axis, so we use the mechanical center of the top box as our reference. If carefully done, the procedure shown here can put the wavefront optical axis within 10-arcsec of the derotator axis. We believe the accuracy could be improved by replacing the rail target "dot" with a crosshair assembly.

NOTE WARNING: *Be sure to cover the intensified CCD cameras so that the laser doesn't accidentally shine on their cathodes and damage them.*

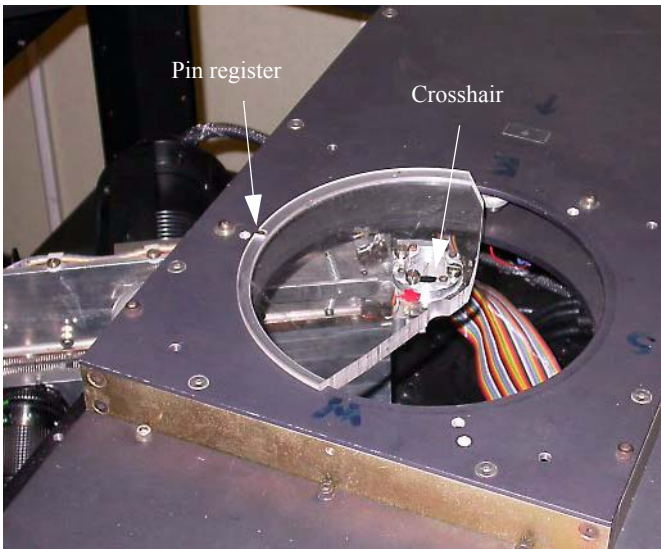


Figure 8: Upper top box crosshair assembly. Care must be taken to register the plexiglass holder in the groove of the shutter assembly and into the pin restriction.

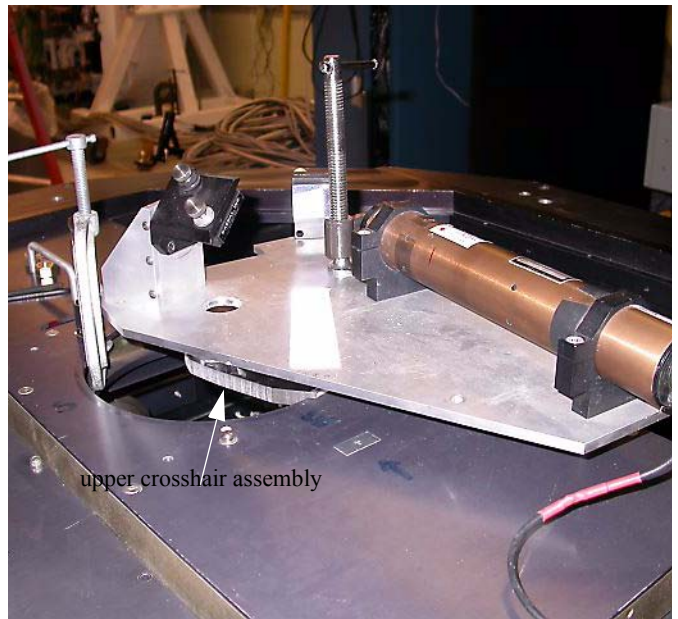


Figure 10: Mount plate holding laser and steering mirrors above the upper crosshair and clamp.

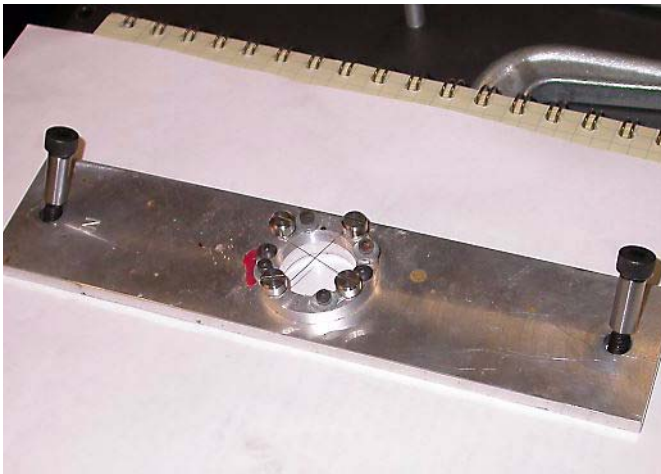


Figure 9: The crosshair assembly mounts into the bottom top box perforation. Note the "N" must correspond to the North of the top box. Be very careful when seating the shoulder bolts as they stick and are hard to see.

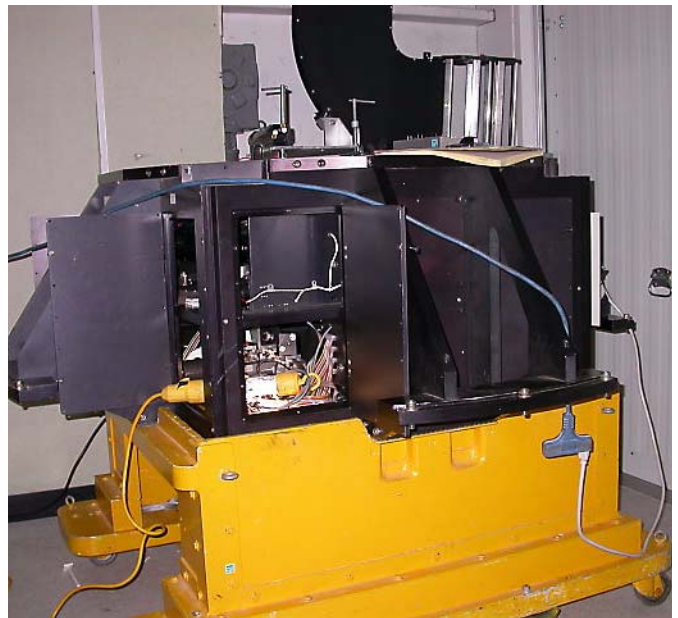


Figure 11: View of the top box with doors open near wavefront sensor for access.

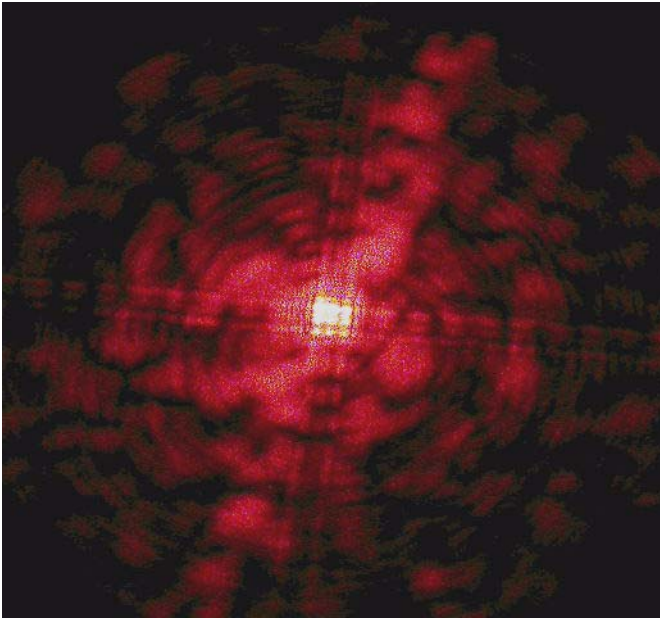


Figure 12: Next, steer laser onto upper crosshair. Adjust until above diffraction pattern is seen (note 9 intensity lobes at center). Remove upper crosshair, and repeat for lower crosshair assembly. Iterate between crosshairs until both diffraction patterns overlay and cross at the center. Now the laser beam is aligned with the top box mechanical axis.

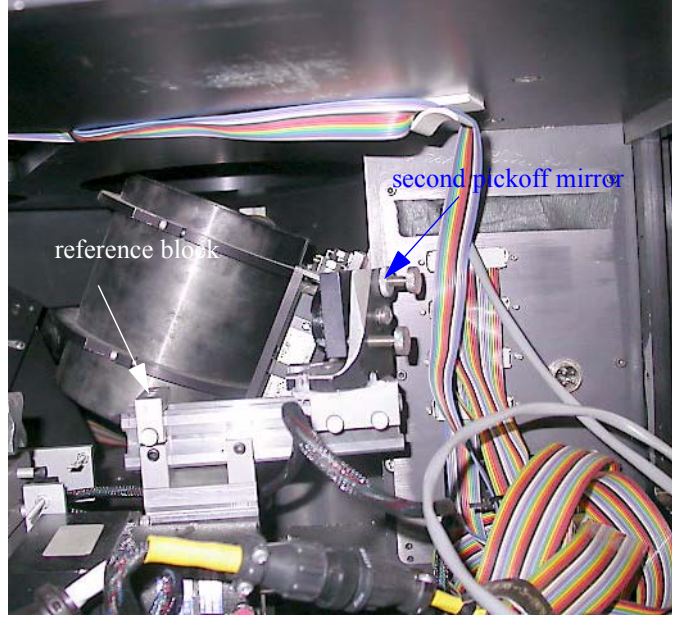


Figure 14: Loosen and move the small steering mirror (in front of the wavefront sensor) away from the reference block (do not loosen or move the reference block as it defines the position of the mirror mount on the slide).



Figure 13: Move in comparison assembly. Snap on mirror cover shown in figure. Laser should intersect target. Remove cover. This is a sanity check that the mirror is positioned properly and that the laser is on-axis.

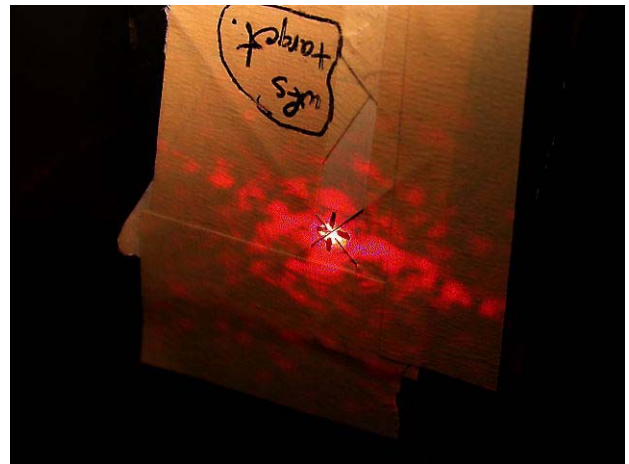


Figure 15: With the second pickoff mirror out of the beam, the laser travels to a target at the corner of the top box. The pickoff mirror above the comparison assembly can now be adjusted until the beam hits the target. This provides for roughly aligning the first mirror independent of anything else in the system. Once finished, move the second mirror to the reference block and lock. The beam is now directed to the wavefront sensor.



## IX. References

- [1] P.L. Schecter, G. Burley, C.L. Hull, M. Johns, B. Martin, S. Schaller, S. A. Shtetman, and S.C. West, "Active Optics on the Baade 6.5-m (Magellan I) Telescope," *Proc. SPIE*
- [2] S.C. West, "Fall 2002 optical performance of the 6.5m MMT analyzed with the top box Shack-Hartmann wavefront sensor," *MMTO Technical Memo #03-1*, January 2003.
- [3] S.C. West and H. Olson, "Baseline Shack-Hartmann design for the 6.5m MMT f/9 focus," *MMTO Technical Memo #01-01*, September 2001.
- [4] S. C. West, S. Callahan, and D. Fisher, "An interferometric Hartmann wavefront analyzer for the 6.5m MMT, and the first results for collimation and figure correction," *MMT Technical Report #37*, (11 June 2001).
- [5] H. M. Martin, S. P. Callahan, B. Cuerden, W. B. Davison, S. T. DeRigne, L/ R. Dettmann, G. Parodi, T. J. Trebisky, S. C. West, and J. T. Williams, "Active supports and force optimization for the MMT primary mirror," in *Advanced Technology Optical/IR Telescopes VI*, L. M. Stepp, ed., *Proc. SPIE* **3352**, 412-423 (1998).
- [6] S. C. West and H. M. Martin, "Correcting 6.5m primary figure errors with the active supports," *MMTO Conversion Technical Memo #00-2*, (18 Jan. 2000).
- [7] L. Noethe, "Active Optics in Modern, Large Telescopes," *Progress in Optics*, 43 (2002).



Figure 16: Remove the optics from the 1:1 reimager optical path, so that the above rail target can be slid along the entire length of the X-26 rail.

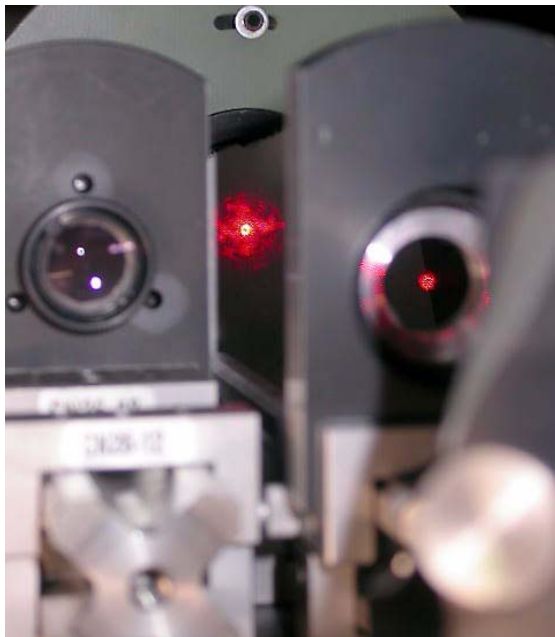


Figure 17: The wavefront channel is shown at left, and the laser is being directed down the re-imager rail at right. Adjust both steering mirrors until the laser remains centered on the rail target at each extreme of the slide. NOTE: The accuracy would be improved by replacing the "dot" with a crosshair and using the diffraction image created by the latter.